Available online at www.sciencedirect.com
SCIENCE DIRECT®
International Journal of Heat and Mass Transfer 47 (2004) 5427–5438
International Journal of HEAT and MASS TRANSFER
www.elsevier.com/locate/ijhmt

Onset of secondary flow and enhancement of heat transfer in horizontal convergent and divergent channels heated from below

C.W. Liu, C. Gau *

Institute of Aeronautics and Astronautics, National Cheng Kung University, Taiwan 70101, ROC

Received 23 September 2003; received in revised form 9 July 2004
Available online 21 September 2004

Abstract

Experiments for the onset and development of the buoyancy driven secondary air flow and enhancement of heat transfer in a horizontal convergent and a divergent channel have been carried out. The bottom wall of the channel is horizontal and heated uniformly, while the top wall is insulated and inclined with respect to the horizontal plane so as to create a convergence angle of 3° for the convergent channel, or a divergence angle of 3° for the divergent channel. The aspect ratio (width to height) and the ratio of channel length to height at the entrance of the channel is 6.67 and 15, respectively. The Reynolds number ranges from 200 to 2000, the buoyancy parameter, Gr/Re^2, from 2.5 to 907 and Pr of the air flow is 0.7. Flow structure inside the channel is visualized by injecting smoke at the inlet flowing along the bottom wall. The onset of secondary flow appearing as transverse instability wave and onset of initial protrusion of the bottom heated layer are identified. Secondary flow structures observed are somewhat different from the case in the parallel-plate channel. This is attributed to the destabilization effect of the deceleration in the divergent channel which results in a much earlier initiation of secondary flow and more pronounced enhancement in the heat transfer, and the stabilization effect of the acceleration in the convergent channel which results in a much later initiation of the secondary flow and less pronounced enhancement in the heat transfer. However, the deceleration flow in the divergent channel and the acceleration in the convergent make the average Nusselt numbers approach the results of the parallel-plate channel. Correlation results for the onset of the secondary flow and enhancement of the heat transfer will be presented and discussed.

1. Introduction

Mixed convection in channels has received great interest in the last three decades for its practical applications in the solar energy collectors, heat exchangers, geothermal energy systems, chemical vapor deposition (CVD) of solid layer in the semiconductor industry, and the cooling of the modern electronic equipments. For horizontal channels heated from below, the buoyancy force can induce secondary flow that appears as mushroom-shaped plumes and vortices, and lead to significant enhancement in the heat transfer. The onset point of the secondary flow is important because it delineates the region before which flow is two-dimensional and pure forced convection heat transfer can be

* Corresponding author. Tel.: +886 6 2757 575; fax: +886 6 2389 940.
E-mail address: gauc@mail.ncku.edu.tw (C. Gau).

0017-9310/$ - see front matter © 2004 Elsevier Ltd. All rights reserved.
doi:10.1016/j.ijheatmasstransfer.2004.07.010

Nomenclature

b	channel height at entrance
g	gravitational acceleration
Gr	Grashof number, $g\beta q(2b)^4/kv^2$
h	convective heat transfer coefficient
$\bar{h}$	average heat transfer coefficient
k	thermal conductivity of air
Nu	local Nusselt number, $h(2b)/k$
$\overline{Nu}$	average Nusselt number, $\bar{h}(2b)/k$
Pr	Prandtl number, v/α
q	heat flux
Ra	Rayleigh number, $GrPr$
Re	Reynolds number defined at the inlet of the channel, $u_o(2b)/v$
T	temperature
u_o	inlet velocity
x,y	coordinate parallel, and normal to the heated wall
X^*	non-dimensional axial distance, $x/(bRePr)$

Greek symbols

β	coefficient of expansion
v	kinematic viscosity

Subscripts

ave	refers to average value
b	refers to bulk mean
o	refers to inlet

assumed. After this region, buoyancy induced secondary flow sets in and the complicated mixed convection flow and its enhancement on the heat transfer has to be considered. It has been found [1,2] that onset of the secondary flow and the enhancement of the heat transfer depends strongly on the Rayleigh number, the Reynolds number, the Prandtl number of the channel flow.

However, in practical applications, the channel may not be in an ideal situation, such as a parallel-plate channel, but a slightly convergent or a divergent channel. For example, in CVD process, the heated susceptor holding the wafers is inclined a small angle with respect to the mainstream to form somewhat like a convergent channel. This is to make a accelerated flow that can lead to a slower rate of boundary layer growth and a relatively more uniform transport process or deposition rate of the solid layer on the wafers. However, this kind of flow configuration has overlooked the onset of buoyancy driven secondary flow that can significantly complicate the transport process. Studies on this kind of transport process in a convergent channel heated from below have been very few [3–5]. The region for the onset of secondary flow and its development with enhancement on the transport process is still not very clear. Since the entire region of the transport process is not clear, there is a question to ask if a slight divergence of the susceptor would be better. In a horizontal parallel-plate channel, however, the onset point was found to approach the leading edge of the heater when the Rayleigh number increases or the Reynolds number decreases. The dimensionless onset point, X^*, has been correlated in terms of a critical Grashof number [6] or Rayleigh number [2]. If the deposition process can be performed before the onset point of the secondary flow, the complicated three-dimensional transport process can be avoided and a relatively uniform deposition of solid film can be obtained.

There are other situations, such as in electronic equipment cooling, one is not clear if a slight divergence or convergence of the channel would make the heat transfer better. Assessment for both the local and the average heat transfer over the entire channel becomes necessary. This need to a complete understanding of the secondary flow process formation and its effect on the heat transfer.

The earlier work on the mixed convection, especially the secondary flow structure and its effect on the heat transfer, was performed primarily in the parallel-plate channel. Mori and Uchida [7] applied the linear stability theory to analyze the fully developed buoyancy induced secondary flow in an asymmetric isothermal channel. Both the first and second type vortex rolls are predicted. Longitudinal convection rolls are observed in the experiments with air which are used to check the validity of the analysis. In the developing region, Hwang and Liu [1] located the onset of thermal instability by observing the longitudinal position at which secondary motion was initiated. The longitudinal station at which the stability was observed was found to be approximately one order of magnitude larger than the prediction based on the linear stability analysis. For the experiments with water,the complete transformation process of the secondary flow from the mushroom shaped plume to the vortices, the breakdown of vortices and the transition to the turbulent flow is visualized [8,9]. The critical Rayleigh numbers for the onset of secondary flow were also studied in the fully developed region [10–12] and the thermal entry region [1,2,6,13]. Correlations for the onset of thermal instability are obtained for both the experiments with water and air. It is found that as the critical Rayleigh number increases or the Reynolds number decreases, the onset of instability moves upstream. Theoretical analysis [14–16] were also performed to predict the onset of the thermal instability. The predictions are close to the experimental

data. For the heat transfer, significant enhancement in the heat transfer due to the secondary flow was found. However, longitudinal periodicity in the Nusselt number upstream of the fully developed region were found only in the experiments with water [8,9], but were not reported in the experiments with air [2,6]. From the review of literature, it appears that the results obtained for the critical Rayleigh number for the initiation of the plume, the number of plume produced and the heat transfer characteristic between the experiments with water and the ones with air are different.

Numerical studies were also performed to study the occurrence and the structure of the secondary flow and the enhancement of heat transfer in both the developing and fully developed regions [17–23]. The trends obtained in general are consistent with the experimental observations. However, most of the numerical calculations assume steady laminar flow. This may not be true for the initiation and growth of the plumes and vortices. Further improvement in the numerical calculation is still needed.

The present paper describes an experimental study for the onset of the buoyancy induced secondary flow and its enhancement in the heat transfer in a horizontal divergent or convergent channel heated from below. A uniform air flow is provided at the entrance, and exits to the ambient after passing through the channel. The bottom wall is maintained in the horizontal position and is heated uniformly. For the divergent (convergent) channel, the opposite, top wall has a divergence (convergence) angle of 3° to the horizontal plane. That is, the downstream end of the top wall is tilted away from (toward) the bottom wall, and is well-insulated. The objective of this investigation is to study and identify the onset and development of the secondary flow and the region for the heat transfer enhancement in a horizontal divergent or a convergent channel. Results of both the flow visualization from the side or the end of the channel by introducing smoke at the inlet, and the heat transfer measurements along the heated wall are presented. It has been found [24–26] that the decelerated flow in the divergent channel has the effect of destabilization on the mainstream while the accelerated flow in the convergent channel has the effect of stabilization. It is interesting to see how the buoyancy induced secondary flow, and the heat transfer will be affected by the decelerated or the accelerated flow in these channels. The effects of the buoyancy parameters and the Reynolds numbers on the flow structures and the Nusselt numbers are reported. Correlations for the onset point of the secondary flow and the heat transfer enhancement will be presented and discussed.

2. Experimental apparatus and procedures

Experiments are performed in a Plexiglas channel, as shown in Fig. 1. The channel is 45 cm in length, 20 cm in width inside and 3 cm in height at the entrance. The heated wall is kept horizontal and the opposite wall is titled with a convergence or divergence angle of 3°. The heated wall is made of 2 cm thick balsa wood and electrically heated. This is achieved by gluing a number of 0.015 cm thick stainless steel foil strips on the entire bottom wall and passing an electric current through the foil heater. DC power is used to provide the electric energy for generating the desired heat flux. The heat flux can be determined by the electric voltage and current passing through the foil. The electric voltage drop due to the contact resistance between the heating strips and the terminals, which connect the heating strips with the DC power supply, has been taken into account. This kind of voltage drop is also noticed in other experiment [27]. For better insulation, a 12 cm thick foamed rubber is glued on the back of the heated wall. All the other side walls are wrapped with 3 cm thick foam rubber.

Since the temperature variation of the heated wall may be large in the transverse direction, the heated wall is instrumented with 7 rows of chromel-alumel thermocouples. One row of the thermocouples is along the centerline of the wall. The distance between two neighboring rows is 2.5 cm, and the spacing between two neighboring thermocouples in each row is 1 cm. Since the surface temperature of the insulated wall is needed for estimating the radiation loss from the heated wall, five additional thermocouples are embedded along the surface of the wall. All thermocouples are calibrated in a constant temperature bath and the measurement error is found to be within ± 0.1 °C. All the temperature signals are acquired with a FLUKE-2287A data logger connected to a computer for direct processing. The temperature data are taken when the entire system reaches steady state, usually in 3–4 h.

During the flow visualization experiments, a smoke generator was used to supply smoke of fine particles. The smoke particles are measured to be in a scale of 2 μm and are small enough to trace the flow in the channel. Smoke enters the channel from a slot of 1 mm width located on the bottom surface in the immediate upstream of the channel entrance, as shown in Fig. 1. A transverse sheet of light perpendicular to the top insulated wall is used to visualize the span wise structure of secondary flow; while the sheet of light from the end parallel to the flow passage is used to visualize the flow structure from the side view. The flow patterns at the upstream, the central and the downstream regions can be observed and recorded. The smoke particles injected were found to have no obvious effect on the heat transfer after rerunning the heat transfer measurements. During the experiments, the flow structure in the channel is sensitive to the circulation of ambient flow. Therefore, a wind shield is constructed around the exit of the channel to prevent this possible extraneous effect.

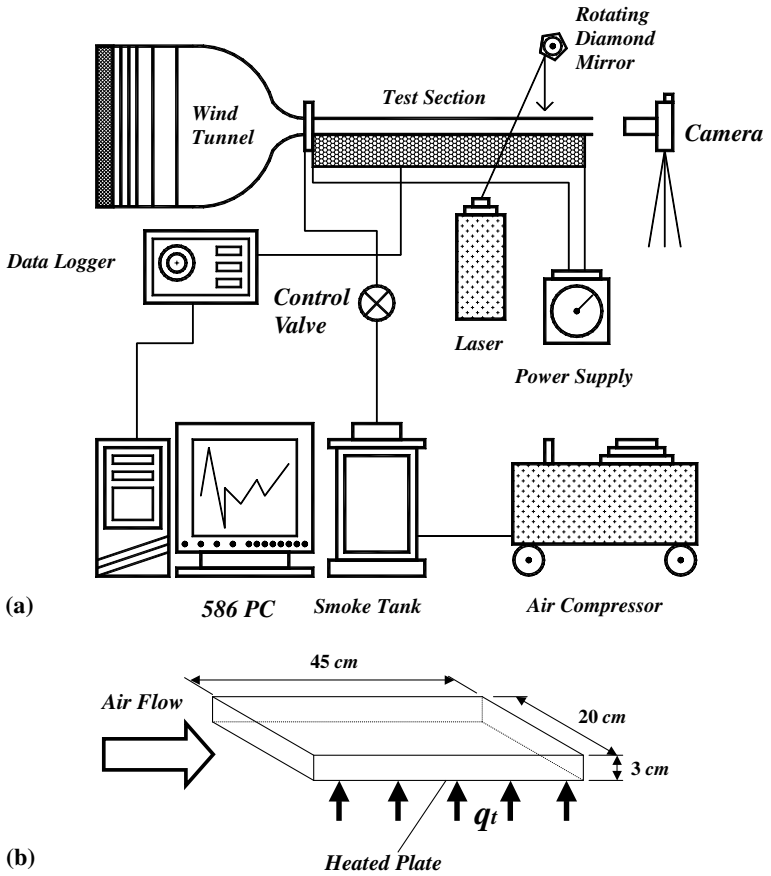

Fig. 1. Schematic diagram of the experimental setup: (1) wind tunnel, (2) smoke tank, (3) power supply, (4) Plexiglas channel, (5) camera, (6) laser, (7) rotating mirror, (8) light source and (9) pumped smoke from smoke generator.

The wind tunnel is the same as the one used in the studies of mixed convection in a heated vertical convergent or divergent channel [3–5]; hence a detailed description is omitted here. The calibration needed for velocity measurement is also described in these reports. The total heat input in a single heating strip can be determined by the electric voltage and current passing through the strip. Since both conduction and radiation losses from each heating strip need to be accounted for and subtracted from the total energy supplied by the heater, the local heat transfer coefficient is evaluated by the following equation:

$$h_r = (q_t - q_{rad} - q_{cond})/(\overline{T}_w - T_r), \quad (1)$$

where $\overline{T}_w$ is the average temperature of a single strip, and r refers to the bulk mean condition or the inlet condition. The conduction loss from the heated wall is estimated by a one-dimensional conduction equation in a composite wall. The procedure to calculate the radiation loss from the heated wall is very similar to the one described in [27] and will not be repeated here. The thermophysical properties used in the local Nusselt number are evaluated at the bulk mean temperature of the flow, while those in the Reynolds and Grashof numbers are evaluated at the inlet temperature.

Since the channel flow exits directly to the ambient, the heat loss is relatively large near the exit. Therefore, the last three heating strips are used only as guard heaters. Relatively large heat loss in the exit region is also found in other experiments [27,28]. The uncertainty of the experimental data is determined according to the procedure proposed by Kline and McClintock [29]. The maximum uncertainty of local Nusselt number is 5.6%, while that for the Reynolds and Grashof number are 6.2% and 7.8%, respectively.

3. Results and discussion

3.1. Flow visualizations

The smoke exits from a spanwise, narrow slot on the bottom wall of the channel at the inlet, and enters smoothly into the channel forming a thin sheet of smoke

along the bottom wall. As the thin-sheet smoke is heated, it becomes unstable and protrudes upward like a plume. The protrusion of plume make the bottom heated layer thinner and cause a higher rate of heat transfer. The plume is found to be initiated from the instability wave as shown in Fig. 2(b) for the parallel-plate channel. The instability wave grows only in amplitude until the wave becomes unstable like small buds, as shown in Fig. 2(c), which lead to protrusion of the flow like fingers, as shown in Fig. 2(d), and become mushroom-shaped plumes at the later stage, as shown in Fig. 2(e). Similar kind of instability wave and plumes can be initiated in the divergent channel, as shown in Fig. 3. However, the divergence of channel can decelerate the flow, at the same time the adverse pressure gradient tends to make the flow unstable. Therefore, due to the destabilization effect of the divergent channel, the instability wave can be initiated at an earlier stage which causes earlier initiation of the plume, as shown in Fig. 3. Part of the reason can be attributed to the deceleration of flow which makes the heated layer thicker, the instability wave can be initiated at an earlier stage.

The secondary flow occurred in divergent channel, as shown in Fig. 3, is somewhat different from the results for parallel-plate channel, as shown in Fig. 2. Due to the destabilization effect of the adverse pressure gradient, the plumes produced is not stable. They oscillate in spanwise direction. In addition, the deceleration of flow can effectively lead to the local increase of Gr/Re^2. Therefore, the mushroom shaped-vortices extend laterally in a more rapid speed than in the parallel-plate channel, which causes interaction with the neighboring vortices and form a complicated flow structure. The interaction of vortices is not observed in the parallel-plate channel for $Re = 500$ and $Gr/Re^2 = 20$, as shown in Fig. 2(f). Since the channel cross section in the downstream is relatively large which gives the plumes more space to grow, the plumes and vortices produced in the divergent channel are greater. The greater plumes produced exhaust more fluid of the heated layer on the bottom wall. This leads to a thinner thermal boundary layer in the bottom which causes a greater enhancement of the heat transfer.

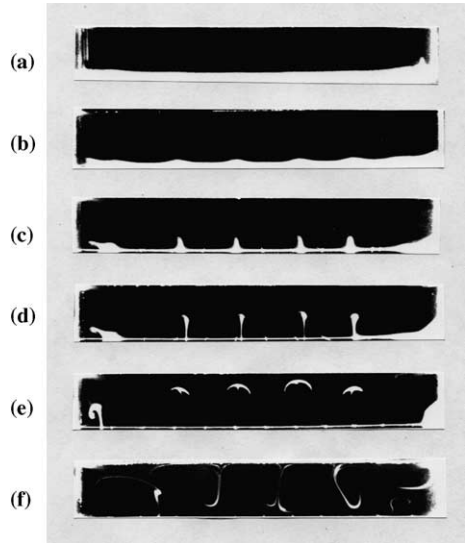

Fig. 2. Flow structure in the parallel-plate channel with $Gr/Re^2 = 20$ and $Re = 500$; (a) $X = 10$ cm, (b) $X = 15$ cm, (c) $X = 20$ cm, (d) $X = 25$ cm, (e) $X = 30$ cm and (f) $X = 44$ cm.

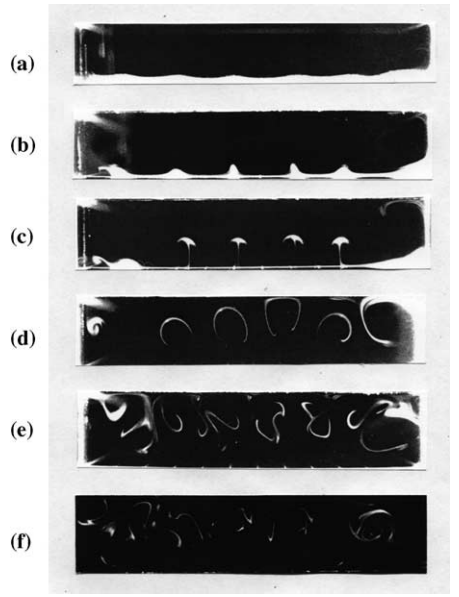

Fig. 3. Flow structure the divergent channel with $Gr/Re^2 = 20$ and $Re = 500$; (a) $X = 10$ cm, (b) $X = 15$ cm, (c) $X = 20$ cm, (d) $X = 25$ cm, (e) $X = 30$ cm and (f) $X = 44$ cm.

As the buoyancy parameter increases, the bottom heated layer becomes thicker. The initiation of plumes and formation of mushroom head occur at a much earlier stage and the number of plumes initiated increases, as shown in Fig. 4. These findings agree with the one reported in [9]. In the downstream, the growth of plume and lateral extension of the mushroom head leads to a strong interaction of vortices, as shown in Fig. 4(d) and (e). Not only that the interaction can occur at an earlier stage but also the interaction is highly unstable and form a very complicated flow structure, as shown in Fig. 4(e). However, no breakdown of vortices and transition to the turbulent flow is found as described in the experiments with water. This is also true within the range covered by the current experiments.

For divergent channel, the appearance of instability wave, formation of fingers or plumes and interaction of neighboring plumes or vortices can occur at an earlier

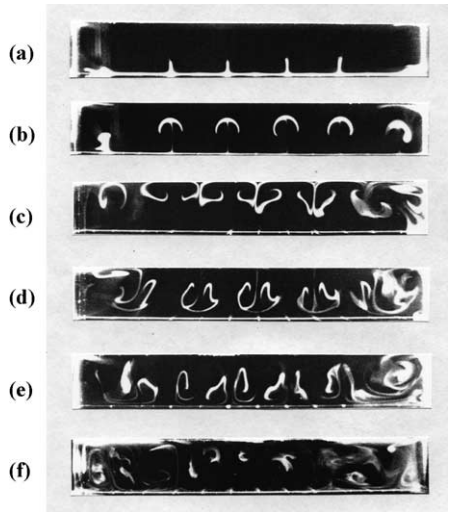

Fig. 4. Flow structure in the parallel-plate channel with $Gr/Re^2 = 60$ and $Re = 500$; (a) $X = 10$ cm, (b) $X = 15$ cm, (c) $X = 20$ cm, (d) $X = 25$ cm, (e) $X = 30$ cm and (f) $X = 44$ cm.

stage than in the parallel-plate channel, as one compares Fig. 4 with Fig. 5. The earlier interaction of plumes leads to a thinner bottom heated layer which can increase the heat transfer. The interaction between plumes or vortices is so severe that the mushroom shaped vortex structure can not be visualized in the downstream region, as shown in Fig. 5(e) and (f). However, the flow is still very steady and laminar, no transition to turbulent flow has occurred. Since the channel height is relatively large in the downstream, this makes the heated fluid smoke to stay in the upper region of the channel.

It is interesting to see how the secondary flow rises and causes the enhancement of the heat transfer along the channel. This can be done by observing the rise of the secondary flow from the side and compare the flow with the measurements of the local Nusselt number distribution along the channel, as shown in Figs. 6–8. There are three different important points, i.e., the onset of the secondary flow, the onset of the heat transfer enhancement and the maximum in the heat transfer, that need to be identified. The onset point of the secondary flow can be located by the appearance of the instability wave. The onset of heat transfer enhancement can be identified at the location, where the Nusselt number has reached minimum and has just started to rise. As contrast to the flow observation, this is the point, where instability wave has become unstable and appeared like small buds, and the thermal has just started to rise. The maximum in the heat transfer occurs at the location, where the plume has been well established and has almost reached the top wall of the channel. One expects that this is the location, where the bottom heated layer has been completely sucked and removed by the plume flow, and heat transfer on the bottom wall reaches maximum. As flow moves downstream, the bottom heated layer can grow thicker again. The growth of the bottom heated layer makes the heat transfer to decrease.

Due to the destabilization effect in the divergent channel, the onset point of the secondary flow, the onset of the heat transfer enhancement and the maximum in

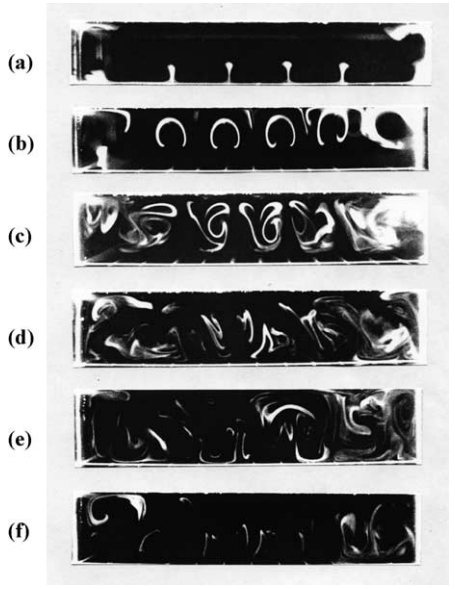

Fig. 5. Flow structure in the divergent channel with $Gr/Re^2 = 60$ and $Re = 500$; (a) $X = 10$ cm, (b) $X = 15$ cm, (c) $X = 20$ cm, (d) $X = 25$ cm, (e) $X = 30$ cm and (f) $X = 44$ cm.

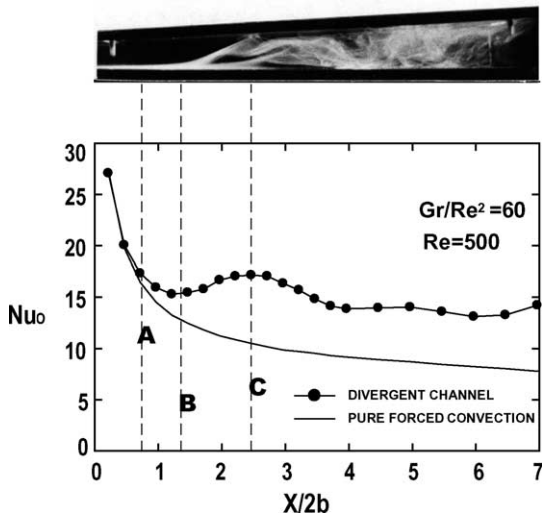

Fig. 6. Side view of the secondary flow in contrast to the local Nusselt number distribution for the divergent channel with $Re = 500$ and $Gr/Re^2 = 60$.

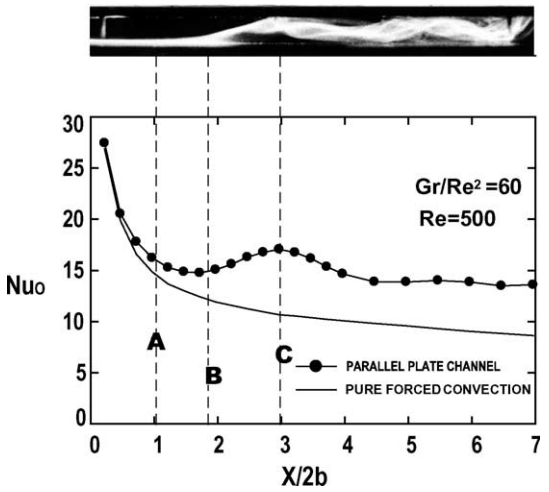

Fig. 7. Side view of the secondary flow in contrast to the local Nusselt number distribution for the parallel-plate channel with $Re = 500$ and $Gr/Re^2 = 60$.

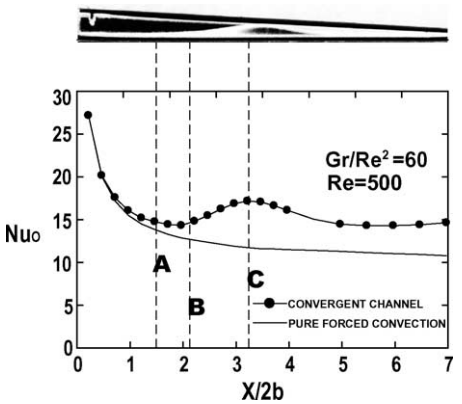

Fig. 8. Side view of the secondary flow in contrast to the local Nusselt number distribution for the convergent channel with $Re = 500$ and $Gr/Re^2 = 60$.

the heat transfer moves upstream. It appears that the onset of the heat transfer enhancement is very sensitive to the divergence of the channel, which moves far upstream close to the onset of the secondary flow, as shown in Fig. 6. This is attributed to the destabilization of the divergent channel. The onset of the heat transfer enhancement is the point, where instability wave becomes unstable and becomes like small buds. This unstable flow can be more affected by the destabilization effect of the divergent channel.

In the convergent channel, the flow acceleration, or the favorable pressure gradient has the effect to stabilize the flow. The plumes produced is smaller and stable. No interaction between neighboring plumes were found [5]. In addition, the acceleration of flow can make the bottom heated layer thinner. This makes both the instability wave and the rise of the bottom heated layer to be initiated at a later stage, as one compares the onset point of the secondary flow and the enhancement in the heat transfer between Fig. 7 for the parallel-plate channel and Fig. 8 for the convergent channel. In addition, it is noted that the rise of the plume must be at the stage when the bottom heated layer becomes and grows thicker enough. However, the acceleration of flow in the convergent channel can make slower the growth rate of the bottom heated layer. Therefore, the rise of the plume can be delayed at a much later stage, as shown in Fig. 8, when the bottom heated layer becomes thicker enough.

3.2. Mixed convection heat transfer

The current heat transfer data was validated by comparing our data in the parallel-plate channel with the results published previously. The agreement was found to be very good [3–5].

As one compares the Nusselt number at $Gr/Re^2 = 60$ and $Re = 500$ between the case of the convergent, as shown in Fig. 8, and the case of the divergent channel, as shown in Fig. 6, the heat transfer enhancement by the secondary flow in the divergent channel is much greater than in the convergent channel. This is attributed to the deceleration of the flow in the divergent channel that the ratio of the buoyancy force versus the inertial force is greater than that in the parallel-plate channel, and the effective value of Gr/Re^2 inside the channel is much greater than 60. In the convergent channel, however, the acceleration of the flow makes the ratio of the buoyancy force versus the inertial force less, and the effective value of Gr/Re^2 inside the channel is much less than 60.

However, as one puts all the Nusselt number results for the parallel-plate, the convergent and the divergent channel into to one figure, as shown in Fig. 9(a), the Nusselt number results for different channels are not much different when the Reynolds number is not large, except that the location of the maximum Nusselt number in the divergent channel is much earlier while in the convergent channel it is much later. In the downstream region, the Nusselt number results for different channels approach each other. However, when the Reynolds number becomes higher, i.e., the forced convection effect becomes stronger, not only all the maxima of the heat transfer for the different channels move downstream, but also the Nusselt number results become deviating largely, as shown in Fig. 9(b). The maximum heat transfer for the convergent channel has moved far downstream that it could not be seen within the range of the current channel.

The deviation in the heat transfer for different channels can be more clearly seen in Fig. 10 for the average

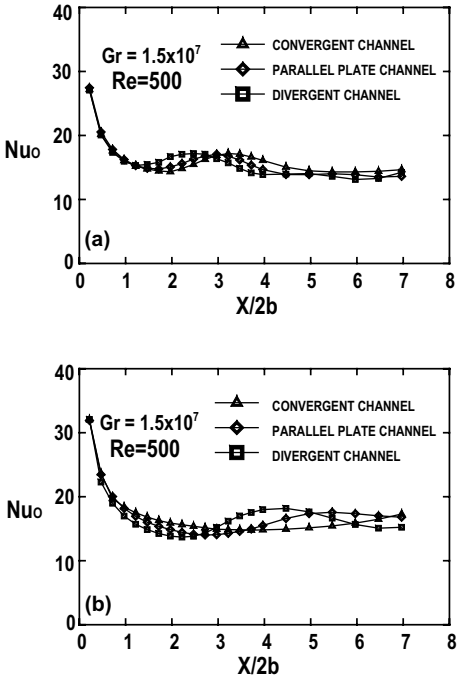

Fig. 9. Comparison of the local Nusselt number distributions among the cases of the divergent, the parallel-plate and the convergent channel for $Gr = 1.5 \times 10^7$ and (a) $Re = 500$ and (b) $Re = 1000$.

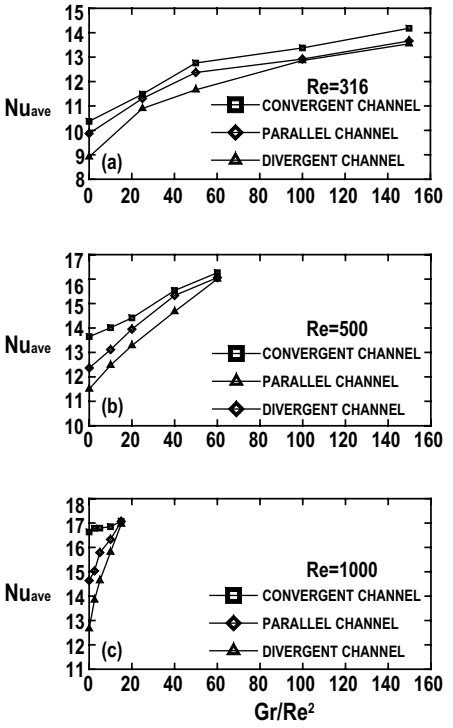

Fig. 10. Buoyancy effect on the average Nusselt numbers for the cases of the divergent, the parallel-plate and the convergent channel at: (a) $Re = 316$, (b) $Re = 500$ and (c) $Re = 1000$.

Nusselt number results. For the case of pure forced convection, the average Nusselt number deviates largely. This is attributed to the acceleration in the convergent channel which can significantly increase the heat transfer, and the deceleration in the divergent channel which can significantly decrease the heat transfer. The greater the Reynolds number, the greater the deviation of the average Nusselt numbers for different channels become. However, as the buoyancy parameter becomes large, the average Nusselt numbers for different channels rapidly approach the case of parallel-plate channel, as shown in Fig 10(c). For smaller Reynolds number, the deviation of the average Nusselt numbers for different channels remains but decreases slightly when the buoyancy parameter increases. This is attributed to the increase of the average Nusselt number in the divergent or the parallel-plate channel due to the increase of the buoyancy parameter is not so rapid as in the case when the Reynolds number is higher. It appears that at the lower Reynolds number condition, the enhancement in the heat transfer due to the buoyancy driven secondary flow in the divergent or the parallel-plate channel is not so large as the case at higher Reynolds number condition. More clear comparison is given numerically in Table 1 for the $Nu_{ave}/(Nu_{ave})_{forced}$ at some Reynolds numbers and $Gr/Re^2 = 15$.

3.3. Onset of secondary flow and heat transfer enhancement

It is very interesting to study how the divergence or the convergence of the channel will affect the onset point of the secondary flow and the heat transfer enhancement by the buoyancy driven flow. The location for the onset of the secondary flow can be identified when the instability wave becomes significant and flow becomes three-dimensional. Before the onset of the secondary flow, the channel flow can be viewed as two-dimensional. The heated layer in the bottom is stable. Up to the onset of the heat transfer enhancement, the buoyancy induced secondary flow has a negligible effect on the heat transfer. Pure forced convection heat transfer results can be adopted before this point. After this point, however, heat transfer enhancement becomes significant and increases until reaching the maximum. This is the region, where buoyancy induced convection has to be considered and chemical vapor deposition application should be avoided. Previous discussion has emphasized that the divergence of channel can cause earlier initiation of the secondary flow due to the destabilization effect while the convergence of channel can delay initiation of this secondary flow due to the stabilization effect. However, one would like to know to what extend the

Table 1
Ratio of $Nu_{ave}/(Nu_{ave})_{forced}$ in the divergent, the parallel-plate and the convergent channels for $Gr/Re^2 = 15$

$Gr/Re^2 = 15$	Re	$Nu_{ave}/(Nu_{ave})_{forced}$
Convergent	316	1.0577
	500	1.0292
	1000	1.0241
Parallel-plate	316	1.0808
	500	1.0887
	1000	1.1644
Divergent	316	1.1112
	500	1.1217
	1000	1.3492

onset point will be affected by the convergence or the divergence of channel.

Correlations for the onset of the secondary flow and the heat transfer enhancement has been performed and obtained in the parallel-plate channel for the thermal entry condition [2]. The Rayleigh number has been selected as the parameter to correlate with a dimensionless distance X^* for the onset point. Therefore, the same correlation parameters were used in the current combined entry flow condition. Successful correlations have been obtained and can be written as follows:

$$Ra = A(X^*)^B, \tag{2}$$

where the constants A and B in the equation are listed in Table 2. Comparison of the current data with the previous results is shown in Fig. 11. Both the onset point for the secondary flow and the heat transfer enhancement in the current combined entry condition agree very well with that in the thermal entry condition. It is noted that the velocity profile at the inlet of the channel is fully developed for the thermal entry condition, but is uniform flow for the combined entry condition. It appears that the instability wave generated in the upstream region is not affected by the velocity boundary layer. In other words, the heated layer in the bottom that causes the instability wave is not affected at all by the shape of the velocity profile across the channel. The initiation of the instability wave is affected only by the buoyancy force that is characterized by the Rayleigh number. Therefore, the Rayleigh number that is selected in the correlation process can adequately describe the instability phenomenon in the system.

After the onset of the heat transfer enhancement, the bottom heated layer protrude into the mainstream and gradually forms mushroom-shaped plumes. The mainstream flow is highly different for the developing and the fully developed condition. In the developing condition, the potential core outside the boundary layer is accelerated by the growth of the wall boundary layer, which can push and drive the bottom heated protrusion flow forward. This action can expedite the suction and removal of the bottom heated layer and cause an earlier contact of the top cold fluid with the wall and significantly enhance the heat transfer. Therefore, the point of the maximum heat transfer for the developing flow condition is initiated significantly earlier than the fully developed flow condition.

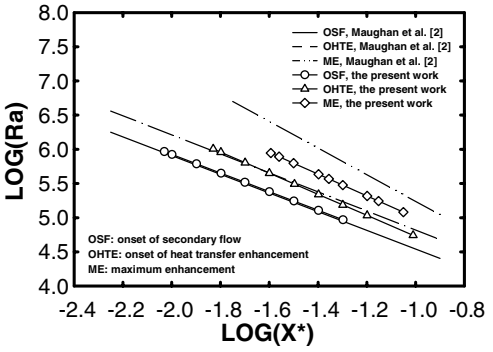

Fig. 11. Correlations for the onset point of secondary flow, the heat transfer enhancement and the maximum point of the heat transfer in the parallel-plate channel, and comparison with the results of others.

Table 2
Correlation Constants for the locations of onset of the secondary flow, the enhancement in the heat transfer and the maximum heat transfer in the divergent, the parallel-plate and the convergent channels

Channels	Locations	A	B
Parallel-plate	Onset of secondary flow	8538.5	−1.39
	Onset of enhancement	7822.4	−1.56
	Maximum heat transfer	10889.3	−1.65
Divergent	Onset of secondary flow	6643.1	−1.33
	Onset of enhancement	2313.6	−1.73
	Maximum heat transfer	1973.1	−1.99
Convergent	Onset of secondary flow	19458.9	−1.29
	Onset of enhancement	7122.5	−1.63
	Maximum heat transfer	43602.3	−1.40

In the divergent channel, however, the destabilization effect due to the adverse pressure gradient can make the small disturbance to grow at a more rapid rate that the instability wave in the bottom heated layer can be initiated at an earlier stage. This can cause the onset point of the secondary flow to move upstream in the divergent channel, as shown in Fig. 12(a). In addition, the earlier initiation of the instability wave in the bottom heated layer causes an earlier initiation of the wave protrusion into the mainstream. This causes the onset of the heat transfer enhancement to move upstream, as shown in Fig. 12(a).

However, the shift of the onset of the heat transfer enhancement to the upstream at the lower Rayleigh number is greater than that at the higher Rayleigh number. It can be seen that the destabilization effect of the divergent channel can make the protrusion of the instability wave more easier to occur at the lower Rayleigh number. Thus, the bottom heated layer at higher Rayleigh number is more unstable than at the lower Rayleigh number. The destabilization effect of the divergent channel does not contribute much to destabilize the bottom heated layer because this layer is already highly unstable and can readily protrude into the mainstream.

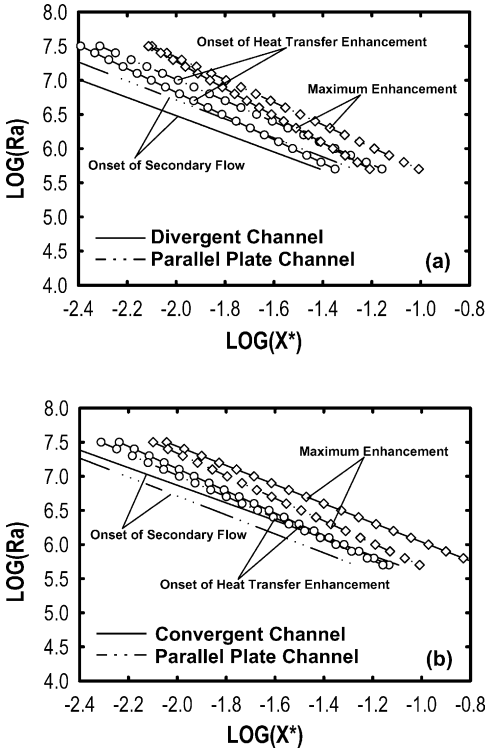

Fig. 12. Comparison and correlations for the onset point of the secondary flow, the heat transfer enhancement and the maximum point of the heat transfer in: (a) the divergent channel and (b) the convergent channel.

However, at lower Rayleigh number the destabilization effect of the divergent channel can more readily disturb the more stable bottom heated layer and make the initial protrusion of the bottom heated layer to occur at much earlier stage. The earlier protrusion of the bottom heated layer causes an earlier formation of the mushroom-shaped plumes that can suck and remove the bottom heated layer and make at an earlier stage the contact of the top cold fluid with the bottom heated wall. Therefore, the divergence of the channel can shift the point of the maximum heat transfer upstream. In addition, the shift to the upstream for the maximum heat transfer is much greater at lower Rayleigh number, while it is much less at higher Rayleigh number. The constants in the correlation equation are also listed in Table 2.

In the convergent channel, the favorable pressure gradient or the acceleration can stabilize or suppress the small disturbance in the flow that the instability wave in the bottom heated layer can be initiated at later stage. This can cause the onset point of the secondary flow to move downstream in the convergent channel, as shown in Fig. 12(b). However, it can be seen that the suppression effect for the instability wave is more significant at a low Rayleigh number than at a high Rayleigh number. The suppression effect can also make the onset point of protrusion of the bottom heated layer to shift to the downstream, as shown in Fig. 12(b).

However, the downstream shift is not so significant as comparison with the case of parallel-plate channel. This leads to the results that at low Rayleigh number conditions the protrusion of the bottom heated layer is initiated once instability wave in this layer occurs. It can be seen that the stabilization effect of the acceleration in the convergent channel does not have much effect on the onset of protrusion of the bottom heated layer, but it does have much effect to shift to the downstream the maximum point of the heat transfer, especially at low Rayleigh number. However, the line for the maximum heat transfer is parallel, and has a similar correspondence to the line for the onset of the secondary flow, as shown in Fig. 12(b). It is very likely that in the convergent channel, it is the suppression of the instability wave that leads to the shift of the maximum heat transfer to the downstream. However, more detailed measurements are needed for clarification. Again, the constants in the correlation have been obtained and are listed in Table 2.

4. Conclusions

Onset of the buoyancy induced secondary flow and the enhancement of heat transfer in a bottom heated horizontal divergent or convergent channel has been

studied. The instability wave for the onset of secondary flow, the initial protrusion of the wave in the bottom heated layer which leads to the onset of heat transfer enhancement can be clearly identified in the current flow visualization experiments. The destabilization effect of the decelerated flow in the divergent channel can make the onset of the secondary flow, the heat transfer enhancement and the point of the maximum heat transfer to be initiated at an earlier stage, while the stabilization effect of the accelerated flow in the convergent channel can make them to be initiated at a later stage. This action leads to a significant variation in the local Nusselt number distributions.

In the divergent channel, the plumes produced are greater and not stable. In addition, the deceleration of flow can effectively lead to the local increase of Gr/Re^2. Therefore, stronger interaction with the neighboring plumes and vortices are observed and form a complicated flow structure. This leads to a greater enhancement in the heat transfer.

In the convergent channel, it is on the contrary. the acceleration of flow can effectively lead to the local decrease of Gr/Re^2. The plumes produced are smaller and stable. No interaction between plumes are found. This leads a less enhancement in the heat transfer. However, the deceleration flow in the divergent channel and the acceleration in the convergent make the average Nusselt numbers approach the results of the parallel-plate channel, especially when the Reynolds number is higher.

Correlations for the onset of the secondary flow, enhancement of the heat transfer and the point of the maximum heat transfer in both the divergent and the convergent channel have been very successful and the results have been discussed and compared with the case of the parallel-plate channel.

Acknowledgment

This research was sponsored by the National Science Council of Taiwan under Contract No. NSC 87-2212-E006-088.

References

[1] G.J. Huang, C.L. Liu, An experimental study of convective instability in the thermal entrance region of a horizontal parallel-plate channel heated from below, Can. J. Chem. Eng. 54 (1976) 521–525.

[2] J.R. Maughan, F.P. Incropera, Regions of heat transfer enhancement for laminar mixed convection in a parallel plate channel, Int. J. Heat Mass Transfer 33 (1990) 555–570.

[3] C. Gau, C.W. Liu, T.M. Huang, W. Aung, Secondary flow and enhancement of heat transfer in horizontal parallel-plate and convergent channels heating from below, Int. J. Heat Mass Transfer 42 (1999) 2629–2647.

[4] C. Gau, T.M. Huang, W. Aung, Flow and mixed convection heat transfer in a divergent heated vertical channel, ASME J. Heat Transfer 108 (1996) 606–615.

[5] C.W. Liu, Mixed convection flow and heat transfer in a heated convergent or divergent channel, M.S. Thesis, National Cheng Kung University, Tainan, Taiwan, 1998.

[6] J.R. Maughan, F.P. Incropera, Experiments on mixed convection heat transfer for airflow in a horizontal rectangular and inclined channel, Int. J. Heat Mass Transfer 30 (1987) 1307–1318.

[7] Y. Mori, Y. Uchida, Forced convection heat transfer between horizontal flat plate, Int. J. Heat Mass Transfer 9 (1966) 803–817.

[8] D.G. Osborne, F.P. Incropera, Laminar, Mixed convection heat transfer for flow between horizontal parallel plates with asymmetric heating, Int. J. Heat Mass Transfer 28 (1985) 207–217.

[9] F.P. Incropera, A.L. Knox, J.R. Maughan, Mixed convection flow and heat transfer in the entry region of a horizontal rectangular duct, ASME J. Heat Transfer 109 (1987) 434–439.

[10] M. Akiyama, G.H. Hwang, K.C. Cheng, Experiments in the onset of longitudinal vortices in laminar forced convection between horizontal plates, ASME J. Heat Transfer 93 (1971) 335–341.

[11] S. Ostrach, Y. Kamotani, Heat transfer augmentation in laminar fully developed channel flow by means of heating from below, ASME J. Heat Transfer 97 (1975) 220–225.

[12] K.C. Chiu, J. Ouazzani, F. Rosenberger, Mixed convection between horizontal plates – II. Fully developed flow, Int. J. Heat Mass Transfer 30 (1987) 1655–1662.

[13] K.C. Chiu, J. Ouazzani, F. Rosenberger, Mixed convection between horizontal plates – I. Entrance effects, Int. J. Heat Mass Transfer 30 (1987) 1645–1654.

[14] F.S. Lee, G.J. Hwang, Transient analysis on the onset of thermal instability in the thermal entrance region of a horizontal parallel-plate channel, ASME J. Heat Transfer 113 (1991) 363–370.

[15] F.S. Lee, G.J. Hwang, The effect of asymmetric heating on the onset of thermal instability in the thermal entrance region of a parallel-plate channel, Int. J. Heat Mass Transfer 34 (1991) 2207–2218.

[16] J.N. Lin, F.C. Chou, P.Y. Tzeng, Theoretical prediction of the onset of thermal instability in the thermal entrance region of horizontal rectangular channels, Int. J. Heat Fluid Flow 12 (1991) 218–224.

[17] M.M.M. Abou-Ellail, S.M. Morcos, Buoyancy effects in the entrance region of horizontal rectangular channels, ASME J. Heat Transfer 105 (1983) 152–159.

[18] H.V. Mahaney, F.P. Incropera, S. Ramadhyani, Development of laminar mixed convection in the thermal entrance region of horizontal rectangular ducts, Num. Heat Transfer 12 (1987) 137–155.

[19] J.R. Maughan, F.R. Incropera, Fully developed mixed convection in a horizontal channel heated uniformly from above and below, Num. Heat Transfer A 17 (1990) 417–430.

[20] F.C. Chou, G.J. Hwang, Vorticity-method for Graetz problem with the effect of natural convection in a

horizontal rectangular channel with uniform wall heat flux, ASME J. Heat Transfer 109 (1987) 704–710.
[21] J.N. Lin, F.C. Chou, Laminar mixed convection in the thermal entrance region of horizontal isothermal rectangular channels, Can. J. Chem. Eng. 67 (1989) 361–367.
[22] T.A. Nyce, J. Ouazzani, A. Durand-Daubin, F. Rosenberger, Mixed convection in a horizontal rectangular channel – Experimental and numerical velocity distributions, Int. J. Heat Mass Transfer 35 (1992) 1481–1494.
[23] C.C. Huang, T.F. Lin, Vortex flow and thermal characteristics in mixed convection of air in a horizontal rectangular duct: effects of the Reynolds and Grashof numbers, Int. J. Heat Mass Transfer 38 (1995) 1661–1674.
[24] C.C. Su, H. Lin, Forced convection in the entrance region of convergent and divergent ducts of rectangular cross section, J. CSME 12 (3) (1991) 314–319.
[25] H. Tanaka, H. Kawamura, A. Tateno, S. Hatamiya, Effect of laminarization and retransition on heat transfer for low Reynolds number flow through a converging to constant area duct, ASME J. Heat Transfer 104 (1982) 363–371.
[26] K.R. Mutama, H. Iacovides, The investigation of developing flow and heat transfer in a long convergent duct, ASME J. Heat Transfer 115 (1993) 897–903.
[27] B.W. Webb, D.P. Hill, High Rayleigh number laminar natural convection in an asymmetrically heated vertical channel, ASME J. Heat Transfer 111 (1989) 649–656.
[28] R.A. Wirtz, P. McKinley, Buoyancy effects on downward laminar convection between parallel-plates, in: Fundamentals of Forced and Mixed Convection, ASME HTD-Vol. 42, 1985, pp. 105–112.
[29] S.J. Kline, F.A. McClintock, Describing uncertainties in single-sample experiments, Mech. Eng. 75 (1953) 3–12.